Nanoscale Advances

PAPER

View Article Online
View Journal | View Issue



Cite this: *Nanoscale Adv.*, 2019, **1**, 757

# Engineering efficient upconverting nanothermometers using $Eu^{3+}$ ions†

Giacomo Lucchini, [a] Adolfo Speghini, *[a] Patrizia Canton, [b] Fiorenzo Vetrone *[cd] and Marta Quintanilla‡[c]

Upconversion nanothermometry combines the possibility of optically sensing temperatures in very small areas, such as microfluidic channels or on microelectronic chips, with a simple detection setup in the visible spectral range and reduced heat transfer after near-infrared (NIR) excitation. We propose a ratiometric strategy based on $Eu^{3+}$ ion luminescence activated through upconversion processes. $Yb^{3+}$ ions act as a sensitizer in the NIR region (980 nm), and energy is transferred to $Tm^{3+}$ ions that in turn excite $Eu^{3+}$ ions whose luminescence is shown to be thermally sensitive. Tridoped $SrF_2$:$Yb^{3+}$,$Tm^{3+}$,$Eu^{3+}$ nanoparticles (average size of 17 nm) show a relative thermal sensitivity of 1.1% $K^{-1}$ at 25.0 °C, in the range of the best ones reported to date for $Ln^{3+}$-based nanothermometers based on upconversion emission. The present nanoparticle design allows us to exploit upconversion of lanthanide ions that otherwise cannot be directly excited upon NIR excitation and that may provide operational wavelengths with a highly stable read out to fill the spectral gaps currently existing in upconversion-based nanothermometry.

Received 31st July 2018
Accepted 1st November 2018

DOI: 10.1039/c8na00118a

rsc.li/nanoscale-advances



## 1. Introduction

The development of all-optical nanoparticle-based thermometers allows for the measurement of localized temperature with a high spatial resolution in sub-millimeter areas, which can serve as a tool for the characterization of microfluidic channels or electronic microcircuit surfaces.[1–3] Particularly interesting are optical luminescent nanothermometers, that, once excited in their absorption region, exhibit a temperature-dependent emission, usually in the ultraviolet (UV), visible or near infrared (NIR) regions. Several parameters related to emission properties can serve as thermal probes, such as intensities, intensity ratios, bandwidths, luminescence lifetimes or band shifts.[4–6] However, not all of them are equally advantageous when it comes to real applications. For instance, using the intensity of a single emission band can be misleading if the concentration of nanoparticles in the area under investigation is not well controlled, since it can create intensity fluctuations not related to temperature but to a different number of emitters. For this reason, it is a good option to analyze parameters that are independent of the concentration of nanoparticles, as is the case with luminescence lifetimes, bandwidths, band intensity ratios or peak shifts.[3] However, from the implementation point of view, the measurement of light intensity presents the advantage of less complex optical setups than lifetime measurements and often has higher sensitivities than bandwidth or peak shift measurements. In the present investigation, a ratiometric technique was proposed to evaluate the temperature,[5] where the intensity of an emission band is used as a reference for a different, separate band, to avoid the mentioned concentration-triggered uncertainty. This luminescence intensity ratio (LIR) offers a further point of reliability also by removing any inaccuracy caused by uncontrolled fluctuations of the excitation light. LIRs are often exploited for lanthanide ($Ln^{3+}$)-based nanothermometers, where several thermally coupled pairs of states have already been investigated and reported in the literature.[7] The emission bands of $Ln^{3+}$ ions are typically narrow and well defined, and this feature permits us to restrict the range in which emission spectra need to be measured to estimate temperature values. Moreover, narrow emission bands facilitate the option of multiplexing, if more than one probe has to be used.

Upconversion (UC) properties shown by several $Ln^{3+}$ ions, *i.e.* generating photons at higher energies with respect to the

[a]*Nanomaterials Research Group, Dipartimento di Biotecnologie, Università di Verona and INSTM, UdR of Verona, Strada Le Grazie 15, I-37314 Verona, Italy. E-mail: adolfo.speghini@univr.it*

[b]*Centro di Microscopia Elettronica "Giovanni Stevanato", Dipartimento di Scienze Molecolari e Nanosistemi, Università Ca' Foscari Venezia, Via Torino 155/B, Venezia-Mestre, Italy*

[c]*Institut National de la Recherche Scientifique, Centre Énergie, Matériaux et Télécommunications (INRS – EMT), Université du Québec, 1650 Boul. Lionel-Boulet, Varennes, QC, J3X 1S2 Canada. E-mail: vetrone@emt.inrs.ca*

[d]*Centre for Self-Assembled Chemical Structures, McGill University, Montreal, QC, H3A 2K6 Canada*

† Electronic supplementary information (ESI) available. See DOI: 10.1039/c8na00118a

‡ Current Address: BioNanoPlasmonics Laboratory, CIC biomaGUNE, Paseo de Miramón 182, 20014 Donostia – San Sebastián (Spain).

excitation radiation, are due to the unique ladder-like arrangement of their 4f energy level states, coupled with the relatively long lifetimes of these levels, typically in the μs or even ms timescales.[8,9] UC has interesting advantages with respect to the usual Stokes emission in the visible range. In fact, the excitation radiation can be chosen in the NIR range, where common solvents, such as water, are poorly absorbing and heat transfer to the sample from the excitation radiation is minimized. Second, UC processes are multiphoton in nature, and therefore they permit a higher spatial resolution due to the non-linear dependence of the emission on the power density of the excitation radiation. Third, since the excitation and the emission radiation are well separated in energy, the emitted radiation can be easily isolated from the excitation radiation. This avoids any interference into the detection system and therefore provides an excellent signal-to-noise ratio, which is further supported by the lack of autofluorescence from additional molecules that might be present in the environment.[10]

One of the most studied upconverting $Ln^{3+}$-based systems for LIR nanothermometry involves $Er^{3+}$ ions co-doped with $Yb^{3+}$ ions, to enhance the harvesting of the excitation light in the NIR region (around 980 nm).[4,7,11] However, previous studies with different materials have demonstrated that alternative $Ln^{3+}$ ions, such as $Dy^{3+}$ ions,[12–14] $Eu^{3+}$ ions[15,16] or $Pr^{3+}$ ions,[17,18] can show better thermal sensitivities, although they are less efficiently excited through upconversion processes.[19] Among these ions, $Eu^{3+}$ is a particularly interesting luminescent probe in fields such as biomedicine,[20] luminescent inks for anti-counterfeiting,[21] and thermometry.[22] However, the $Eu^{3+}$ energy level structure does not permit UC emission by directly exciting with NIR radiation in the biological window (700–1200 nm), due to lack of resonant energy levels. Nonetheless, with sufficient codoping with $Yb^{3+}$ ions, that are sensitizers of NIR excitation radiation at 980 nm, $Eu^{3+}$ ions can show UC in the visible.[23] A population of the excited states of $Eu^{3+}$ ions can be obtained through a simultaneous energy transfer from two different $Yb^{3+}$ ions to an $Eu^{3+}$ ion, a cooperative process that has relatively low probability.[24,25] On the other hand, other $Ln^{3+}$ ions, for instance $Tm^{3+}$, with energy levels resonant with those of $Eu^{3+}$, could help in populating $Eu^{3+}$ levels through energy transfer processes and therefore dramatically improve UC emission.[26,27] Following these considerations, with the target of exploiting $Eu^{3+}$ ion UC for nanothermometry while allowing for NIR excitation, we chose a triple doping strategy ($Yb^{3+}$, $Tm^{3+}$, $Eu^{3+}$), implemented in water dispersible $SrF_2$ nanoparticles in the colloidal form, which have been shown to be excellent hosts for UC luminescence and easily prepared in particle sizes as small as 15 nm.[28]

# 2. Experimental

## 2.1 Nanoparticle preparation

$Tm^{3+}$, $Yb^{3+}$ and $Eu^{3+}$-tridoped $SrF_2$ upconverting nanoparticles (UCNPs) were synthesized following a hydrothermal method.[29] Briefly, $SrCl_2 \cdot 6H_2O$, $YbCl_3 \cdot 6H_2O$, $TmCl_3 \cdot 6H_2O$ and $EuCl_3 \cdot 6H_2O$ (Aldrich, 99.9%) were used as metal precursors (with $Sr^{2+} : Yb^{3+} : Eu^{3+} : Tm^{3+} = 0.745 : 0.220 : 0.030 : 0.005$ as the nominal molar ratio). As a reference sample, $Yb^{3+}$ and $Eu^{3+}$-codoped $SrF_2$ nanoparticles (with $Sr^{2+} : Yb^{3+} : Eu^{3+} = 0.750 : 0.220 : 0.030$ as the nominal molar ratio) were synthesized following the same procedure and are denoted as $SrF_2$:Yb,Eu nanoparticles. Stoichiometric amounts of the metal chlorides (3.5 mmol of total metal ions) were dissolved in 7 mL of deionized water. This solution was then added to 25 mL of a 0.8 M sodium citrate dihydrate solution (Fluka, >99%) and 3.0 mL of a 3.5 M $NH_4F$ solution (Aldrich, 99.9%). The obtained solution was heat treated at 190 °C for 6 hours in a stainless-steel Teflon-lined digestion pressure vessel (DAB-2, Berghof). Subsequently, the UCNPs were precipitated with acetone and directly dispersed in deionized water. The colloidal dispersion is stable for at least one month.

## 2.2 Experimental setup

**2.2.1 Structural and morphological investigation.** X-ray powder diffraction (XRPD) measurements were carried out with a Thermo ARL X'TRA powder diffractometer equipped with a Cu-anode X-ray source with a Peltier Si(Li) cooled solid state detector. Before the measurements, the samples were homogenized in a mortar with few drops of ethanol. After evaporation of the ethanol, the sample was deposited on a low background sample stage.

TEM (HRTEM) images were obtained using a JEOL 3010 high resolution electron microscope (0.17 nm point-to-point resolution at the Scherzer defocus), operated at 300 KV, equipped with a Gatan slow-scan CCD camera (model 794) and an Oxford Instruments EDS microanalysis detector (Model 6636). The powder was dispersed in water in order to be deposited on holey-carbon copper grids.

**2.2.2 Spectroscopy measurements.** Emission spectra (spectral resolution of 5 $cm^{-1}$) were measured using a 980 nm laser diode (MDLIII980, CNI) as the excitation source and a half meter monochromator (Sr-500i, ANDOR) equipped with a CCD camera (DU420A-BVF, ANDOR) as the recording setup. Emission spectra at different temperatures were recorded by heating the solution with a thermal bath and measuring the temperature with a K-type thermocouple (0.2 °C sensitivity).

# 3. Results and discussion

The X-ray diffraction pattern (shown in Fig. S1, ESI†) shows that the prepared UCNPs have a cubic fluorite phase, as reported for similar nanoparticles.[28] EDX measurements clearly indicate the presence of $Yb^{3+}$ and $Eu^{3+}$, while $Tm^{3+}$ ions are present at a concentration below the limit of detection of the EDX setup (Fig. S2, ESI†). Nonetheless, the presence of $Tm^{3+}$ ions is clearly demonstrated by the strong UC emission (see below). A representative TEM micrograph of the UCNPs is shown in Fig. 1a, presenting a nice dispersion and average particle size of 16 nm (see Fig. 1b).

Upon laser excitation at 980 nm, a large number of emission bands in the near UV, blue and red optical regions are observed for the $SrF_2$:$Yb^{3+}$,$Tm^{3+}$,$Eu^{3+}$ UCNPs[28,30–32] as shown in Fig. 2. After 980 nm laser excitation, several $Tm^{3+}$ excited states can be populated following energy transfer processes from $Yb^{3+}$ to

 

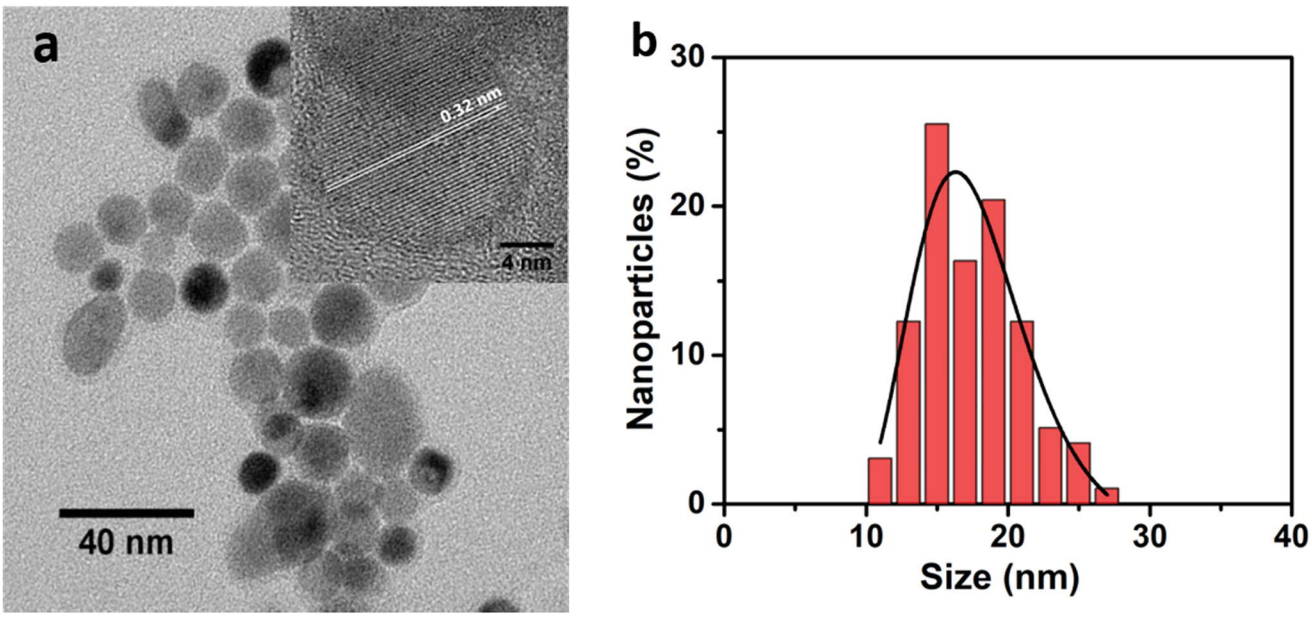


Fig. 1 (a) Representative TEM image of the $SrF_2$:$Yb^{3+}$, $Tm^{3+}$, $Eu^{3+}$ UCNPs. Inset: HRTEM image showing the (111) lattice planes. (b) Particle size distribution calculated using Pebbles software and log-normal fit (average particle size: 16 ± 4 nm).

$Tm^{3+}$ ions, as described by grey dashed arrows in Fig. 3a. Several emission bands are thus related to transitions from different $Tm^{3+}$ excited states either to the ground state ($^3H_6$) or to lower lying excited states (see blue labels in Fig. 2).

In addition, a group of less intense bands in the 400–440 nm and 500–630 nm regions are nicely observed, as shown in Fig. 2b and S3 (ESI†), typical of emission of $Eu^{3+}$ ions, which constitutes clear evidence of the population of the excited energy levels of $Eu^{3+}$ ions through upconversion processes. The transition assignments for the observed bands have been carried out considering the spectroscopic investigation of Jouart *et al.*[33] and Cortelletti *et al.*[39] for $Eu^{3+}$ centres in $SrF_2$ using site-selective excitation techniques.

In principle, an $Yb^{3+}$ → $Eu^{3+}$ cooperative upconversion process could be present.[23,34–36] Nonetheless, the $SrF_2$:Yb,Eu NPs, prepared as a reference, without $Tm^{3+}$ ions, do not show any $Eu^{3+}$ upconversion emission upon 980 nm laser excitation under the same experimental conditions (see Fig. S4, ESI†). Therefore, the $Eu^{3+}$ upconversion emission found for the tri-doped $SrF_2$:$Yb^{3+}$,$Tm^{3+}$,$Eu^{3+}$ NPs clearly indicates that a $Tm^{3+}$ → $Eu^{3+}$ energy transfer is involved and it is active once the excited levels of $Tm^{3+}$ ions have been populated by the $Yb^{3+}$ → $Tm^{3+}$

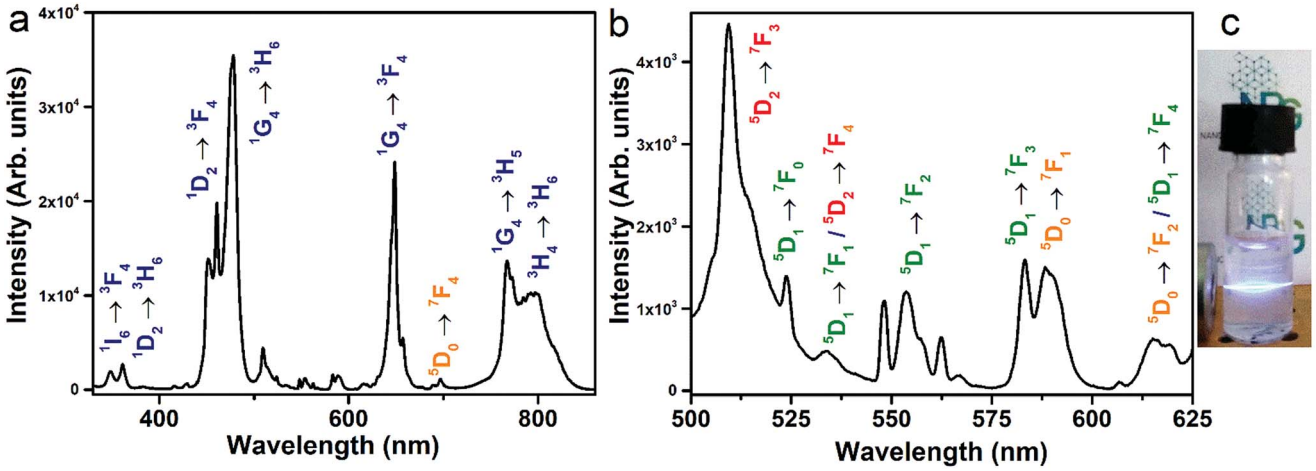


Fig. 2 (a) Upconversion emission of a water colloidal dispersion of the $SrF_2$:$Yb^{3+}$,$Tm^{3+}$,$Eu^{3+}$ UCNPs (1 wt%, dopant percentage: $Yb^{3+}$ 22%, $Tm^{3+}$ 0.5%, and $Eu^{3+}$ 3%) after laser excitation at 980 nm (power density of 450 mW $mm^{-2}$). (b) Same as (a) in the 500–650 nm range. Blue: $Tm^{3+}$ ion transitions. Orange: $Eu^{3+}$ ion transitions from the $^5D_0$ level. Green: $Eu^{3+}$ ion transitions from the $^5D_1$ level. Red: $Eu^{3+}$ ion transition from the $^5D_2$ level. (c) Picture of the $D_2O$ colloidal dispersion of the $SrF_2$:$Yb^{3+}$,$Tm^{3+}$,$Eu^{3+}$ UCNPs (concentration of 1 wt%) after laser excitation at 980 nm (power density of 450 mW $mm^{-2}$).

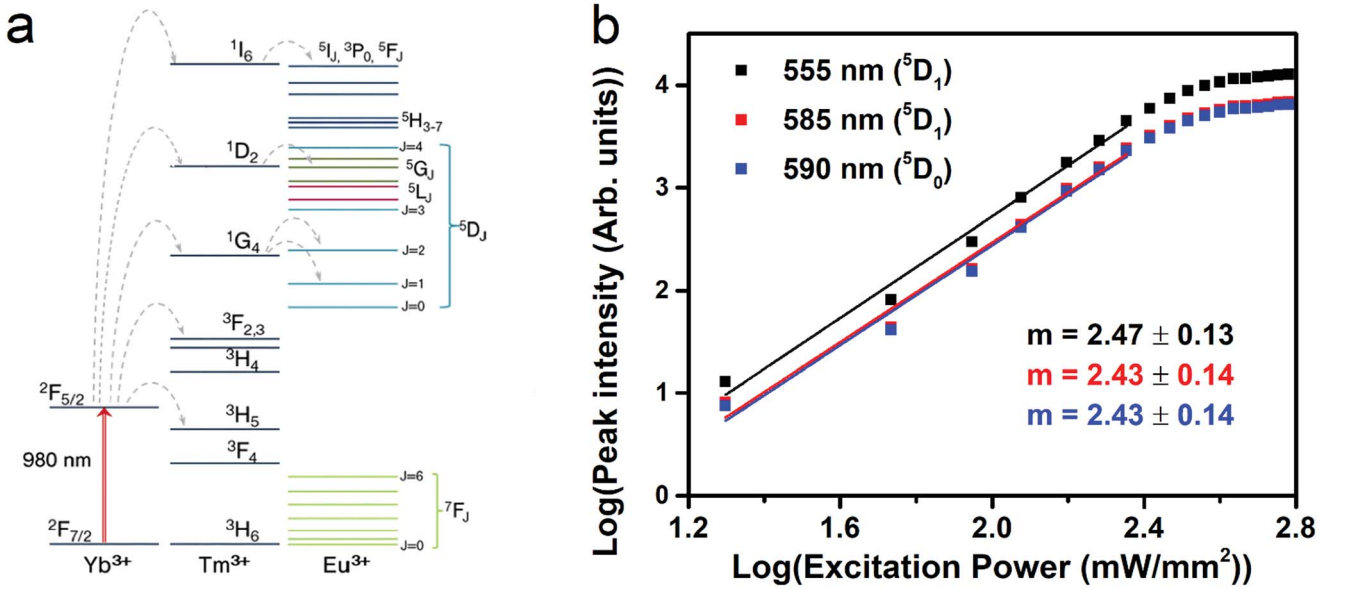


Fig. 3 (a) Energy level scheme for $Yb^{3+}$, $Tm^{3+}$ and $Eu^{3+}$ ions, $Yb^{3+}$ excitation (red arrow) and energy transfer processes (grey dashed arrows). (b) Power study of several $Eu^{3+}$ upconversion bands of the $SrF_2$:$Yb^{3+}$,$Tm^{3+}$,$Eu^{3+}$ UCNPs upon 980 nm laser excitation at 25 °C.

upconversion. The population of $Eu^{3+}$ energy levels by means of excited $Tm^{3+}$ ions is already reported in the literature.[37,38] From an inspection of the energy levels of the $Tm^{3+}$ ions, energy transfer processes responsible for the $Eu^{3+}$ energy level population are sketched in Fig. 3. It is interesting to note that the $Eu^{3+}$ emission bands shown in the upconversion spectra (see Fig. 2b) have very different relative intensities than those observed in Stokes $Eu^{3+}$ emission spectra of $SrF_2$:$Eu^{3+}$ nanoparticles upon direct excitation of the $Eu^{3+}$ excited energy levels, as reported by Cortelletti *et al.*[39] This different behavior can be explained considering the different pathways populating the $Eu^{3+}$ excited levels, which in the present case are fed through $Tm^{3+} \rightarrow Eu^{3+}$ energy transfer processes. A similar $Tm^{3+}$ to $Eu^{3+}$ energy transfer process has also been observed for tridoped Eu,Tm,Yb lithium lanthanide phosphate nanoparticles, after excitation at 975 nm with a diode laser.[27]

Some weak emission bands observed in the blue region around 415 and 430 nm correspond to emissions from the $^5D_3$ level of the $Eu^{3+}$ ions, indicating that an energy transfer process from the $^1D_2$ level of $Tm^{3+}$ to the $^5D_4$, $^5G_J$ or $^5L_J$ levels of $Eu^{3+}$ is present. A contribution to the population of the $Eu^{3+}$ excited levels could be in principle also due to an energy transfer process from the $^1I_6$ level of $Tm^{3+}$, as emission from this level is observed in the UC spectrum (see Fig. 2). Nonetheless, it is reasonable to consider this contribution as much less relevant with respect to those due to energy transfer starting from the lower lying $^1D_2$ and $^1G_4$ excited energy levels of $Tm^{3+}$ ions. This behavior is due to the much lower population of the $^1I_6$ level with respect to the other two levels, evidenced by the very low relative intensity of the $^1I_6 \rightarrow {}^3F_4$ band (see Fig. 2a). Moreover, the energy of the $^1G_4$ level of $Tm^{3+}$ ions is slightly higher than that of the $^5D_1$ level of $Eu^{3+}$ ions; thus a $Tm^{3+}(^1G_4) \rightarrow Eu^{3+}(^5D_1)$ energy transfer process is reasonably present, with possible phonon emission. A $Tm^{3+}(^1G_4) \rightarrow Eu^{3+}(^5D_2)$ energy transfer process can also be possible considering that the $Tm^{3+}(^1G_4)$ and $Eu^{3+}(^5D_2)$ levels are almost resonant, with small phonon absorption assistance.

The upconversion mechanisms described in Fig. 3a, therefore, play a fundamental role in populating the $Eu^{3+}$ energy levels. In order to investigate the power dependence of the $Eu^{3+}$ upconverted luminescence, UC spectra were measured as a function of the 980 nm laser power density (between 20 and 500 mW mm$^{-2}$), and they are shown in Fig. 3b. The peak intensities for the different transitions follow a log–log behavior for laser powers up to ~190 mW mm$^{-2}$, and then a saturation behavior is observed. The slopes, denoted as $m$, associated with each transition were evaluated in the linear regime, as they are related to the number of photons involved in the upconversion process. The $m$ values are much higher than 2, indicating that a three-photon process is present and therefore suggesting that the population of the $Eu^{3+}$ energy levels is mainly from energy transfer from the $^1G_4$ level of $Tm^{3+}$ ions. We point out that the $Eu^{3+}$ upconversion is observable with our experimental setup for laser powers (at 980 nm) as low as 20 mW mm$^{-2}$ (2 W cm$^{-2}$), a value that is comparable with those employed to generate upconversion for similar water-dispersible nanoparticles.[40] It is important to note that as transitions starting from $^5D_2$, $^5D_1$ and $^5D_0$ energy levels of $Eu^{3+}$ show the same power dependency, any intensity ratio between emissions originating from these levels is independent of the excitation power, a paramount property for a reliable luminescence thermometric system. The non-radiative relaxation probability of the $^5D_J$ ($J = 0, 1, 2$) levels is in principle different, due to the different energy gaps between each level and the next lying one,[28,41] and therefore the relative intensities of the emission bands could vary on changing the temperature. In addition, the energy transfer mechanisms from $^1G_4$ ($Tm^{3+}$) to the $^5D_1$ ($Eu^{3+}$) is non-resonant (see Fig. 3) and thus, dependent on the phonon density of states. The UC

 

spectra of the $SrF_2$:$Yb^{3+}$,$Tm^{3+}$,$Eu^{3+}$ UCNPs were measured as a function of temperature in the 20–60 °C range. Representative examples are shown in Fig. 4a, from which it can be noted that the $Eu^{3+}$ emission bands in the 580–600 nm range show a notable relative variation on changing the temperature. We define the LIR as

$$\mathrm{LIR} = \frac{A(^5D_0 \rightarrow {}^7F_1)}{A(^5D_1 \rightarrow {}^7F_3)} \quad (1)$$

where $A$ denotes an integrated emission of the corresponding transition, as evidenced by shaded areas in Fig. 4a. As shown in Fig. 4b, the LIR shows a monotonically increasing behavior on increasing the temperature in the investigated range (20–60 °C). In order to evaluate possible variations of the LIR with the laser excitation power, we have measured a series of upconversion spectra at increasing power densities, and the results are shown in Fig. 4c. Very importantly, from these results, we demonstrate that the LIR value is independent of the laser excitation power in the range of 200–600 mW $mm^{-2}$ (see Fig. 4c). From the $Eu^{3+}$ upconversion bands (shown in Fig. 2), it can be deduced that the $^5D_1$ and $^5D_0$ states are separated by an energy gap around 1800 $cm^{-1}$, a value consistent with that found for $SrF_2$:$Eu^{3+}$-based samples by site-selective spectroscopy.[33,39] The fact that the LIR shows a growing trend on increasing the temperature and not a decreasing one indicates that the $^5D_1$ and $^5D_0$ states are not thermally linked, but their population depends on the $Tm^{3+} \rightarrow Eu^{3+}$ energy transfer process, shown in Fig. 3a, and subsequent non-radiative processes. The relative sensitivity, $S_r$, of a thermometer, a commonly accepted parameter to compare the performances of different thermometers,[4] is defined as

$$S_r = \frac{1}{\mathrm{LIR}}\left(\frac{\partial \mathrm{LIR}}{\partial T}\right) \quad (2)$$

The $S_r$ values as a function of temperature are shown in Fig. S5† and are determined to be between 0.8 and 1.1% $K^{-1}$ in the 20–60 °C temperature range, with a percentage error of 5%. These values are among the highest reported in the literature for upconverting nanothermometers, as reported in Table 1.[7] The performance of a thermometer is also characterized by another important parameter, that is the minimum temperature uncertainty, $\Delta T_{min}$, which determines the accuracy of the temperature measurements that can be achieved under the working conditions of the thermometer,[4] defined as

$$\Delta T_{min} = \frac{\Delta \mathrm{LIR}}{\mathrm{LIR} S_r} \quad (3)$$

where ΔLIR represents the experimental uncertainty of the LIR. The average value of $\Delta T_{min}$ is evaluated to be 1.9 ± 0.2 °C. It is important to mention that the uncertainty parameter ΔLIR depends on the instrumental setup of the experiments through the signal to noise ratio, and thus it can be improved with a longer integration time, higher laser excitation or better detection equipment.

This value is consistent with those found for similar upconverting thermometers.[42] In order to better understand the physical mechanism governing the behavior of the upconversion emission as a function of temperature, the $SrF_2$:$Yb^{3+}$,$Tm^{3+}$,$Eu^{3+}$ UCNPs were dispersed in $D_2O$ as the solvent, at a concentration of 1 wt%, similar to the one used for experiments with $H_2O$ as the solvent. These dispersions turned out to be colloidally stable for some weeks (see Fig. S6†). It is worth mentioning that the vibrational energy cutoff for the $D_2O$ molecule is 2500 $cm^{-1}$, a value that is much less than that for the $H_2O$ molecule (highest vibrational energy around 3600 $cm^{-1}$)[43]

For this reason, multiphonon relaxation processes for lanthanide ions are much more probable if they are close to $H_2O$ molecules than for $D_2O$ ones, as the higher the vibrational energy is, the larger is the multiphonon relaxation probability of the $Ln^{3+}$ excited level. We show in Fig. 5a the comparison between upconversion spectra of the $SrF_2$:$Yb^{3+}$,$Tm^{3+}$,$Eu^{3+}$ UCNPs using $H_2O$ and $D_2O$ as dispersing solvents, while using identical experimental conditions with respect to the geometrical setup and in particular the same power density of the laser excitation radiation. From Fig. 5a, it can be noted that in the

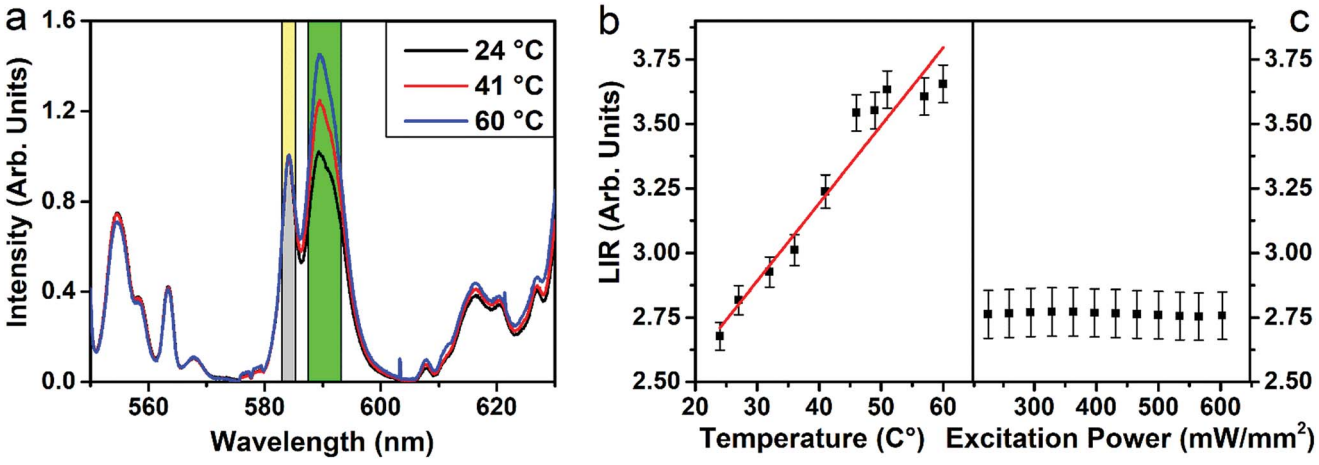


Fig. 4 (a) Emission spectra of the $SrF_2$:$Yb^{3+}$,$Tm^{3+}$,$Eu^{3+}$ UCNPs at three different temperatures (intensity normalized to the 585 nm band) upon 980 nm excitation. (b) Luminescence intensity ratio, LIR = $A(^5D_0 \rightarrow {}^7F_1)/A(^5D_1 \rightarrow {}^7F_3)$ *vs.* T. (c) LIR *vs.* laser excitation power.

Table 1 Relative sensitivity values for upconverting nanothermometers, based on the luminescence intensity ratiometric (LIR) technique

| Host | Dopants | Average particle size (nm) | Excitation wavelength (nm) | Emission range (nm) | $S_r$@25 °C (% $K^{-1}$) | Ref. |
|---|---|---|---|---|---|---|
| ZnO | $Er^{3+}$ | 80 | 978 | 535–555 | 0.5 | 44 |
| $NaYF_4$ | $Er^{3+}$, $Yb^{3+}$ | 6000 | 980 | 530–555 | 1.2 | 45 |
| $NaY(WO_4)_2$ | $Er^{3+}$, $Yb^{3+}$ | 3000 | 980 | 530–550 | 1.0 | 46 |
| $LiNbO_3$ | $Er^{3+}$, $Yb^{3+}$ | 100 | 980 | 525–550 | 0.7 | 47 |
| $CaF_2$ | $Er^{3+}$, $Yb^{3+}$ | 11 | 920 | 522–538 | 1.9 | 42 |
| $GdVO_4$ | $Er^{3+}$, $Yb^{3+}$ | 3.9 | 980 | 525–555 | 1.1 | 48 |
| $LiLaP_4O_{12}$ | $Eu^{3+}$, $Tm^{3+}$, $Yb^{3+}$ | 40 | 975 | 450–700 | 0.34 | 27 |
| $SrF_2$ | $Eu^{3+}$, $Tm^{3+}$, $Yb^{3+}$ | 17 | 980 | 585–590 | 1.1 | This work |

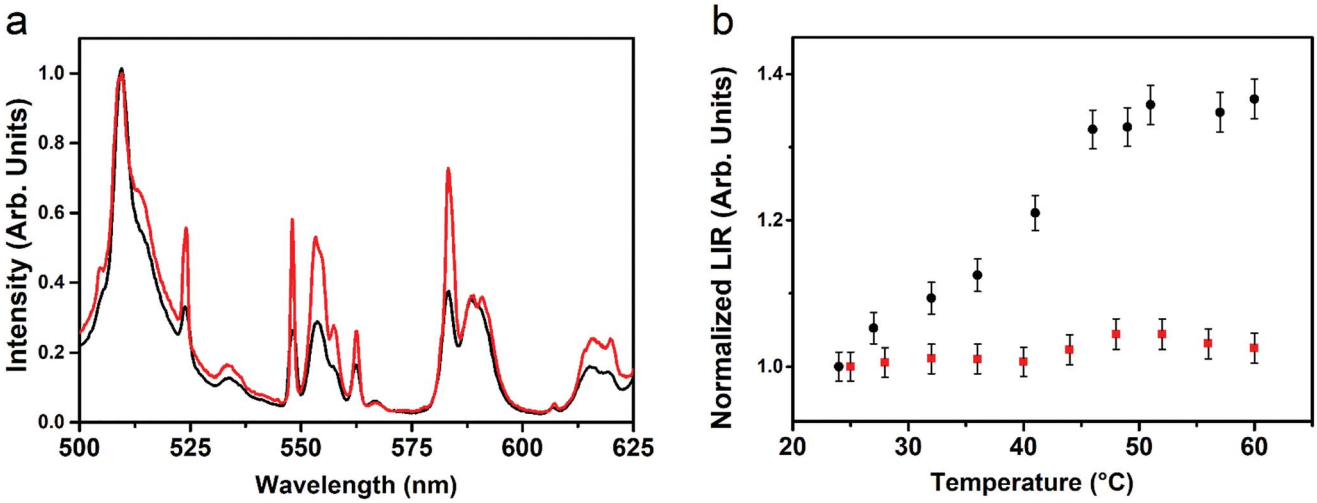


Fig. 5 (a) $Eu^{3+}$ upconversion for $SrF_2$:$Yb^{3+}$,$Tm^{3+}$,$Eu^{3+}$ UCNPs dispersed in $H_2O$ (black line) and in $D_2O$ (red line). (b) LIR for $H_2O$ (black squares) and $D_2O$ (red solid circles)-dispersed UCNPs.

case of $D_2O$ dispersions, the $Eu^{3+}$ upconversion bands corresponding to transitions starting from the $^5D_1$ level are more intense than for those starting from the $^5D_0$ one. The upconversion spectra for $D_2O$ dispersions as a function of temperature (20–60 °C) do not change notably on increasing the temperature (see Fig. S7†), suggesting that the populations of the $^5D_0$ and $^5D_1$ levels of the $Eu^{3+}$ ions do not change significantly with the temperature, at least in the investigated range. The LIR for the $D_2O$ dispersed UCNPs shows an almost constant value (around 1.0), within the experimental uncertainties, on increasing the temperature (Fig. 5b). Such a behavior indicates that the relaxation channel for the $^5D_1$ level is much more effective in $H_2O$ dispersions than in $D_2O$ ones. This behavior is clear evidence that a significant number of $Ln^{3+}$ ions lie on the nanoparticle surface, close to the solvent molecules, as their emission properties are much influenced by the solvent vibrational energies, inducing non-radiative multiphonon relaxation channels. The depopulation of the $^5D_1$ energy level of $Eu^{3+}$ is much more influenced by multiphonon relaxations than that of the $^5D_0$ one, due to a much lower energy gap with the lower lying energy level ($^5D_1$–$^5D_0$, energy gap around 1800 $cm^{-1}$; $^5D_0$–$^7F_6$, energy gap around 12 000 $cm^{-1}$). Therefore, the multiphonon relaxation probability for the $^5D_1$ level is almost constant in the relatively small investigated temperature range for $D_2O$ dispersions, while it is increased for $H_2O$ dispersions, due to the much higher vibrational energy of $H_2O$ with respect to $D_2O$.

The obtained thermometric values for the $SrF_2$:-$Yb^{3+}$,$Tm^{3+}$,$Eu^{3+}$ UCNPs demonstrate that the strategy applied to excite the $Eu^{3+}$ ions offers good opportunities for thermometry in three aspects. First, a careful selection of $Ln^{3+}$ dopants allows us to engineer a mechanism that exploits upconversion to excite $Eu^{3+}$ ions. Second, the different upconversion paths used to excite several $Eu^{3+}$ states allow the definition of a luminescence intensity ratio that remains unaffected during measurements, also for variations of the laser excitation power. Finally, the thermal sensitivity of such an intensity ratio is on par with the best upconverting nanothermometers reported to date.

## 4. Conclusions

In the present study, we investigated colloidal upconverting nanothermometers based on $Yb^{3+}$, $Tm^{3+}$ and $Eu^{3+}$ ions that exploit the matching of the $Tm^{3+}$ ion energy levels with the ones of $Eu^{3+}$ ions. This property permits us to transfer the absorbed energy by the antenna $Yb^{3+}$ ions to the final probe, $Eu^{3+}$ ions. The developed nanothermometer shows a very good relative sensitivity, around 1% $K^{-1}$ in the 20–60 °C range, among the highest values shown by the most popular lanthanide-based

 

nanothermometers. Moreover, the relative sensitivity is independent of intensity fluctuations of the excitation radiation owing to the characteristics of the designed upconversion process. Very importantly, this excitation strategy constitutes a new way of engineering upconversion-based nanothermometers that exploit new ions and that are able to operate at different wavelengths.

## Conflicts of interest

There are no conflicts to declare.

## Acknowledgements

University of Verona (Italy) is gratefully acknowledged for financial support in the framework of the "Ricerca di base 2015" project. F. V. is grateful for financial support from the Natural Sciences and Engineering Research Council (NSERC) of Canada and the Fonds de recherche du Québec – Nature et technologies (FRQNT). P. Canton is grateful for financial support from Ca' Foscari University of Venice ADIR-2016.

## Notes and references

1 L. Aigouy, G. Tessier, M. Mortier and B. Charlot, *Appl. Phys. Lett.*, 2005, **87**, 184105.
2 A. Benayas, B. del Rosal, A. Pérez-Delgado, K. Santacruz-Gómez, D. Jaque, G. A. Hirata and F. Vetrone, *Adv. Opt. Mater.*, 2015, **3**, 687–694.
3 B. del Rosal, E. Ximendes, U. Rocha and D. Jaque, *Adv. Opt. Mater.*, 2017, **5**, 1600508.
4 D. Jaque and F. Vetrone, *Nanoscale*, 2012, **4**, 4301–4326.
5 C. D. S. Brites, P. P. Lima, N. J. O. Silva, A. Millán, V. S. Amaral, F. Palacio and L. D. Carlos, *Nanoscale*, 2012, **4**, 4799–4829.
6 X. Wang, O. S. Wolfbeis and R. J. Meier, *Chem. Soc. Rev.*, 2013, **42**, 7834–7869.
7 M. González-Béjar and J. Pérez-Prieto, *Methods Appl. Fluoresc.*, 2015, **3**, 42002.
8 F. Auzel, *Chem. Rev.*, 2004, **104**, 139–173.
9 J.-C. G. Bünzli and S. V Eliseeva, *Chem. Sci.*, 2013, **4**, 1939–1949.
10 L. Y. Ang, M. E. Lim, L. C. Ong and Y. Zhang, *Nanomedicine*, 2011, **6**, 1273–1288.
11 A. Sedlmeier, D. E. Achatz, L. F. Fischer, H. H. Gorris and O. S. Wolfbeis, *Nanoscale*, 2012, **4**, 7090–7096.
12 Z. Boruc, M. Kaczkan, B. Fetlinski, S. Turczynski and M. Malinowski, *Opt. Lett.*, 2012, **37**, 5214.
13 Z. Cao, S. Zhou, G. Jiang, Y. Chen, C. Duan and M. Yin, *Curr. Appl. Phys.*, 2014, **14**, 1067–1071.
14 M. G. Nikolić, D. J. Jovanović and M. D. Dramićanin, *Appl. Opt.*, 2013, **52**, 1716.
15 J. Rocha, C. D. S. Brites and L. D. Carlos, *Chem.–Eur. J.*, 2016, **22**, 14782–14795.
16 C. D. S. Brites, P. P. Lima, N. J. O. Silva, A. Millán, V. S. Amaral, F. Palacio and L. D. Carlos, *J. Lumin.*, 2013, **133**, 230–232.
17 Y. Gao, F. Huang, H. Lin, J. Zhou, J. Xu and Y. Wang, *Adv. Funct. Mater.*, 2016, **26**, 3139–3145.
18 W. Tang, S. Wang, Z. Li, Y. Sun, L. Zheng, R. Zhang, B. Yang, W. Cao and M. Yu, *Appl. Phys. Lett.*, 2016, **108**, 61902.
19 V. K. Rai, *Appl. Phys. B*, 2007, **88**, 297–303.
20 S. S. Syamchand and G. Sony, *J. Lumin.*, 2015, **165**, 190–215.
21 J. Andres, R. D. Hersch, J. E. Moser and A. S. Chauvin, *Adv. Funct. Mater.*, 2014, **24**, 5029–5036.
22 S. H. Zheng, W. B. Chen, D. Z. Tan, J. J. Zhou, Q. B. Guo, W. Jiang, C. Xu, X. F. Liu and J. R. Qiu, *Nanoscale*, 2014, **6**, 5675–5679.
23 R. Martín-Rodríguez, R. Valiente, S. Polizzi, M. Bettinelli, A. Speghini and F. Piccinelli, *J. Phys. Chem. C*, 2009, **113**, 12195–12200.
24 V. Jubera, A. Garcia, J. P. Chaminade, F. Guillen, J. Sablayrolles and C. Fouassier, *J. Lumin.*, 2007, **124**, 10–14.
25 W. Strek, P. J. Deren, A. Bednarkiewicz, Y. Kalisky and P. Boulanger, *J. Alloys Compd.*, 2000, **300**, 180–183.
26 G. H. Dieke, *Spectra and Energy Levels of Rare-earth Ions in Crystals*, Wiley, New York, 1968.
27 L. Marciniak, A. Bednarkiewicz and W. Strek, *J. Lumin.*, 2017, **184**, 179–184.
28 M. Quintanilla, I. X. Cantarelli, M. Pedroni, A. Speghini and F. Vetrone, *J. Mater. Chem. C*, 2015, **3**, 3108–3113.
29 M. Pedroni, F. Piccinelli, T. Passuello, S. Polizzi, J. Ueda, P. Haro-Gonzalez, L. M. Maestro, D. Jaque, J. Garcia-Sole, M. Bettinelli and A. Speghini, *Cryst. Growth Des.*, 2013, **13**, 4906–4913.
30 F. W. Ostermayer, J. P. Van der Ziel, H. M. Marcos, L. G. Van Uitert and J. E. Geusic, *Phys. Rev. B*, 1971, **3**, 2698.
31 M. Quintanilla, N. Nuñez, E. Cantelar, M. Ocaña and F. Cusso, *Nanoscale*, 2011, **3**, 1046–1052.
32 R. A. Hewes and J. F. Sarver, *Phys. Rev. B: Condens. Matter Mater. Phys.*, 1969, **182**, 427–436.
33 J. P. Jouart, C. Bissieux, G. Mary and M. Egee, *J. Phys. C Solid State Phys.*, 1985, **18**, 1539.
34 Y. Li, J. Guo, X. Liu, T. Aidilibike and W. Qin, *Phys. Chem. Chem. Phys.*, 2016, **18**, 16094–16097.
35 H. S. Wang, C. K. Duan and P. a Tanner, *J. Phys. Chem. C*, 2008, **112**, 16651–16654.
36 G. S. Maciel, A. Biswas and P. N. Prasad, *Opt. Commun.*, 2000, **178**, 65–69.
37 L. Wang, X. Xie, F. Shi, D. Zhao, D. Zhang, K. Zheng, G. Wang, C. He, R. Kim and W. Qin, *Opt. Lett.*, 2009, **34**, 2781–2783.
38 H. Lin, D. Q. Chen, Y. L. Yu, A. P. Yang, R. Zhang and Y. S. Wang, *Mater. Res. Bull.*, 2012, **47**, 469–472.
39 P. Cortelletti, M. Pedroni, F. Boschi, S. Pin, P. Ghigna, P. Canton, F. Vetrone and A. Speghini, *Cryst. Growth Des.*, 2018, **18**, 686–694.
40 M. Pedroni, F. Piccinelli, T. Passuello, S. Polizzi, J. Ueda, P. Haro-Gonzalez, L. M. Maestro, D. Jaque, J. Garcia-Sole, M. Bettinelli and A. Speghini, *Cryst. Growth Des.*, 2013, **13**, 4906–4913.
41 S. Tanabe, S. Yoshii, K. Hirao and N. Soga, *Phys. Rev. B*, 1992, **45**, 4620–4625.

42 N. N. Dong, M. Pedroni, F. Piccinelli, G. Conti, A. Sbarbati, J. E. Ramírez-Hernández, L. M. Maestro, M. C. Iglesias-De La Cruz, F. Sanz-Rodriguez, A. Juarranz, F. Chen, F. Vetrone, J. A. Capobianco, J. G. Solé, M. Bettinelli, D. Jaque and A. Speghini, *ACS Nano*, 2011, **5**, 8665–8671.
43 S. E. Lappi, B. Smith and S. Franzen, *Spectrochim. Acta, Part A*, 2004, **60**, 2611–2619.
44 D. M. Blake, P. C. Maness, Z. Huang, E. J. Wolfrum, J. Huang and W. A. Jacoby, *Sep. Purif. Methods*, 1999, **28**, 1–50.
45 S. Zhou, K. Deng, X. Wei, G. Jiang, C. Duan, Y. Chen and M. Yin, *Opt. Commun.*, 2013, **291**, 138–142.
46 H. Zheng, B. Chen, H. Yu, J. Zhang, J. Sun, X. Li, M. Sun, B. Tian, S. Fu, H. Zhong, B. Dong, R. Hua and H. Xia, *J. Colloid Interface Sci.*, 2014, **420**, 27–34.
47 M. Quintanilla, E. Cantelar, F. Cusso, M. Villegas and A. C. Caballero, *Appl. Phys. Express*, 2011, **4**, 22601.
48 T. V. Gavrilović, D. J. Jovanović, V. Lojpur and M. D. Dramićanin, *Sci. Rep.*, 2014, **4**, 1–9.